3-D wave-equation imaging of a North Sea dataset: common-azimuth migration + residual migration

Louis Vaillant, Stanford University, Henri Calandra, Elf Aquitaine, Paul Sava and Biondo Biondi, Stanford University*

SUMMARY

3-D prestack common-azimuth depth migration (CAM) has strong potential for accurately imaging complex media and correctly handling multi-pathing. Here, we apply the technique to a North Sea dataset recorded over a salt dome region. The results obtained demonstrate the suitability of the method for complex media, and illustrate important differences with Kirchhoff methods. A detailed analysis of associated angle-domain common-image gathers shows opportunities for improving the velocity model.

INTRODUCTION

Wave-equation migration techniques have enjoyed a renewed interest since the shortcomings of Kirchhoff migration are becoming apparent (O'Brien and Etgen, 1998). Moreover, powerful computing resources now make 3-D prestack depth migration feasible with such techniques. Based on a recursive extrapolation of the recorded wavefield, wave-equation migration methods are potentially better able to handle multi-pathing problems induced by complex velocity structures. Thus, they offer an attractive alternative to Kirchhoff methods (Mosher et al., 1997; Biondi, 1997). Additionally, finite frequency wave propagation is modeled avoiding asymptotic approximations.

Common-azimuth migration (CAM) is a 3-D prestack depth migration technique based on the wave equation (Biondi and Palacharla, 1996). It exploits the intrinsic narrow-azimuth nature of marine data to reduce its dimensionality and thus manages to cut the computational cost of 3-D imaging significantly enough to compete with Kirchhoff methods.

Elf Aquitaine provided us with an interesting dataset recorded in the North Sea, which shows a salt dome and other 3-D structures. The complexity of the wave propagation in the medium, resulting from high lateral and longitudinal velocity contrasts, yields multipathing and illumination problems, which makes this model both a serious challenge for imaging and an interesting test case for the common-azimuth migration method.

PREPROCESSING AND MIGRATION

The wave-equation approach obliges to transform the 3-D data acquired with complex irregular geometry to regularly space-sampled data, because CAM operates in the frequency-wavenumber domain and requires Fourier transforms along all axes. In contrast, Kirchhoff algorithms can handle irregular geometries without such preprocessing.

Data regularization is performed by an operator called AMO or Azimuth Moveout (Biondi et al., 1998). It also allows local coherent stack in order to reduce data volume. AMO, however, has a nonnegligible computational cost in the whole imaging process (about 10% of migration cost). With less accuracy, one can instead use a simple normalized binning procedure.

The processing scheme begins by creating a 5-axis time-midpoint-offset grid $(t,\vec{m},\vec{h})$ for the data volume. Then, we apply a simple sequence NMO/AMO/NMO^{-1} to regularize the data. This gridding procedure concurrently allows data resampling in common-midpoint and offset at the limit of aliasing, in order to reduce further the cube dimensions and lower computational cost.

Marine data are usually concentrated within a narrow range of azimuth, as opposed to land data. AMO sums data coherently over the cross-line offset axis h_y. Conventionally, the subscripts x and y refer to the in-line and the cross-line direction, respectively. Thus, we obtain 4-D common-azimuth data, for which $h_y = 0$. After transformation to the frequency-wavenumber domain, this 4-D common-azimuth regularized dataset $D(\omega,\vec{k_m},k_{hx})$ is the wavefield recorded at depth $z = 0$, to which CAM is applied.

Migration is then performed iteratively through common-azimuth downward-continuation of the wavefield (Biondi and Palacharla, 1996). The common-azimuth downward-continuation operator is derived from the stationary-phase approximation of the full 3-D prestack downward continuation operator. For more accuracy with lateral velocity variations, we use several reference velocities and interpolation as in the extended split-step method (Stoffa et al., 1990). The following chart summarizes the preprocessing and imaging schemes:

$$\begin{aligned}
\widetilde{D}_{irr}(t) &= \text{Gridding} \Rightarrow & \widetilde{D}\left(t,\vec{m},\vec{h}\right)\\
\widetilde{D}\left(t,\vec{m},\vec{h}\right) &= \text{AMO} \Rightarrow & D(t,\vec{m},hx)\\
D_{z=0}\left(\omega,\vec{k_m},k_{hx}\right) &= \text{Down} \Rightarrow & D_z\left(\omega,\vec{k_m},k_{hx}\right)\\
D_z\left(\omega,\vec{k_m},k_{hx}\right) &= \text{Imaging} \Rightarrow & D_z\left(\tau=0,\vec{m},h_x=0\right)
\end{aligned}$$

APPLICATION TO REAL DATA

Data characteristics

The migrated volume covers an area of 10.5×4km, down to 5.0km. The velocity model, courtesy of Elf Aquitaine, was obtained by reflection tomography using the SMART method (Jacobs et al., 1992). For migration, we used 6 reference velocities in the extended split-step scheme of CAM. With data dimensions indicated in Table 1, the 3-D prestack common azimuth migration ran in 40 days on 4 processors of our SGI Power Challenge (18 MIPS R8000 processors).

Table 1: number of samples

Cmp-X	Cmp-Y	Depth	Offset	Frequencies	Velocities
525	160	400	64	176	6

Figure 1 shows a typical set of sections in the middle of the migrated cube. In the in-line section, the shallower part (above 1500m) reveals high-frequency details accurately imaged: the migration enhanced a graben structure, with normal faults and rocked blocks, around location Cmp-X=8000m, close to the top. The horizontal section at depth 900m highlights complex patterns inside sedimentary layers, imaged with a high resolution, that can be interpreted as turbidite channels. The imaging of the salt body is satisfactory, with sediments clearly bent towards the salt flank on the left-hand side. The salt flank itself has not been well focused, but can be revealed by residual migration, as discussed later. Even with an imperfect velocity model, migration enhances deep layers and most of the bottom of the salt. Several layers below the salt are also well focused.

Angle-domain common-image gathers

Seismic imaging can be sketched as a two-step process: velocity estimation and migration. All modern migration algorithms require simple and reliable ways to extract prestack information for

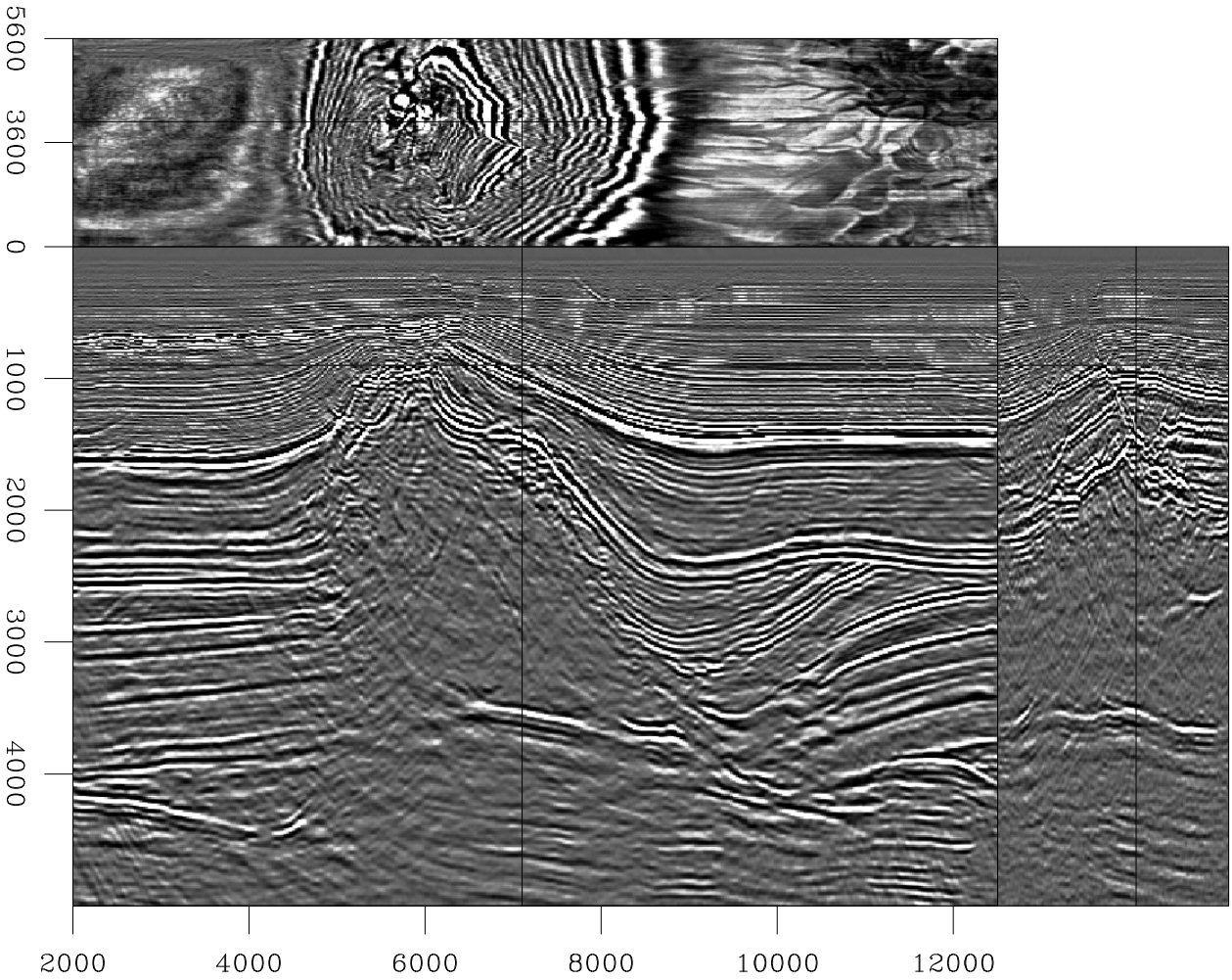

Figure 1: Sections of the migrated cube: in-line Cmp-Y=4000m (center), depth slice z=900m (top), cross-line at Cmp-X=7100m (side).

velocity estimation and updating. For this purpose, angle-domain common-image gathers can be easily computed in the wavenumber domain from the output of CAM (Prucha et al., 1999). Those panels enhance valuable information for analysis when the velocity model is complex and induces multi-pathing.

Figure 2 shows the in-line section at Cmp-Y=3250m, with examples of the angle-domain common-image gathers that can be obtained from the migrated image. Unlike the image in Figure 1, the section is not a stack over the angle axis but instead a near-angle image. Even if it increases the noise level, it also displays more events that are not stacked coherently when the velocity model is not perfect.

The analysis of common-image gathers shows that the velocity model needs further improvements around the salt body. Performing accurate imaging, especially deep in the model, requires a precise relocation of the major reflectors, such as the salt edges, with respect to the velocity model.

For this purpose, the information provided by the common-image gathers can be reinvested in a residual migration process to improve the focusing of the migrated sections. The next step, which is less straightforward, is to update the velocity model from the perturbation between the starting and the improved images (Biondi and Sava, 1999).

Image enhancement by Stolt residual migration

Recent studies (Stolt, 1996; Sava, 2000) have shown that Stolt residual migration can be applied in the prestack domain, as a velocity-independent process. Therefore, it can be used as a tool for enhancing image focusing after CAM without making assumptions about the original velocity model.

By Stolt residual migration, we obtain images that correspond to velocities that have a given ratio to the original one. The process enables flattening the common-image gathers and allows energy to move laterally, as opposed to standard moveout scans (Figure 2).

Figure 3 illustrates the application of Stolt residual migration with a particular ratio. The reflector at the center of the image is made more continuous and appears clearly as the salt flank. Similarly, the continuity of sedimentary layers on its left-hand side is also improved.

As show in Figure 3, a given velocity ratio can improve part of the image but deteriorate the imaging in other regions, like the bottom of salt or the right-hand side salt flank in our example. To generate an image globally improved by residual migration, a set of images corresponding to different ratios is computed and optimal values are picked at every point in the cube.

COMPARISON WITH KIRCHHOFF MIGRATION

Figures 4 and 5 show comparisons between CAM and Kirchhoff migration results. Kirchhoff images are courtesy of Elf Aquitaine. The algorithm used is derived from a preserved-amplitude approach and selects the most energetic arrival. Both CAM and Kirchhoff migration use the same velocity model.

The in-line sections around the salt body are relatively comparable in quality (Figure 4). Globally, CAM seems to give better results at imaging sediments bending against the salt flank on the left-hand side. The most important differences are shown by the horizontal sections (Figure 5): at a depth of 900m, CAM enhances complex high-frequency turbiditic patterns in shallow layers. At the same location, the Kirchhoff image appears considerably lower frequency and blurred along the in-line direction.

There are potentially 3 factors that could explain CAM relative improvement in accuracy compared to Kirchhoff. First, wave propagation is handled completely differently: CAM iteratively propagates the wavefield by regular depth steps, as opposed to Green functions for Kirchhoff. Second, Kirchhoff algorithms usually include critical interpolations of Green functions that may reduce high-frequency accuracy in the image. Third, even if Kirchhoff algorithms can easily handle irregular geometries, the resulting image incorporates acquisition footprints, especially in depth slices. On the contrary, CAM requires regular geometry and acquisition problems are addressed during preprocessing through the AMO operator. Thus, the whole imaging stage is done with regularized geometry and potentially enables higher resolution in the final image.

CONCLUSION

Real data offer an opportunity to test our imaging techniques further. Common-azimuth migration (CAM) is an attractive method for seismic imaging in complex media and it remains a subject for further research. Its computational cost and its high resolution in depth slices, illustrated in this particular example, can make it an attractive alternative to widespread Kirchhoff methods. The imaging of the North Sea data reveals complex lithologic structures. Angle-domain common-image gathers highlight imaging insufficiencies around the steepest parts of salt flanks. They also offer opportunities for residual migration and velocity estimation.

ACKNOWLEDGEMENTS

The authors would like to thank Elf Aquitaine for providing the data and the velocity model, as well as the Kirchhoff images.

REFERENCES

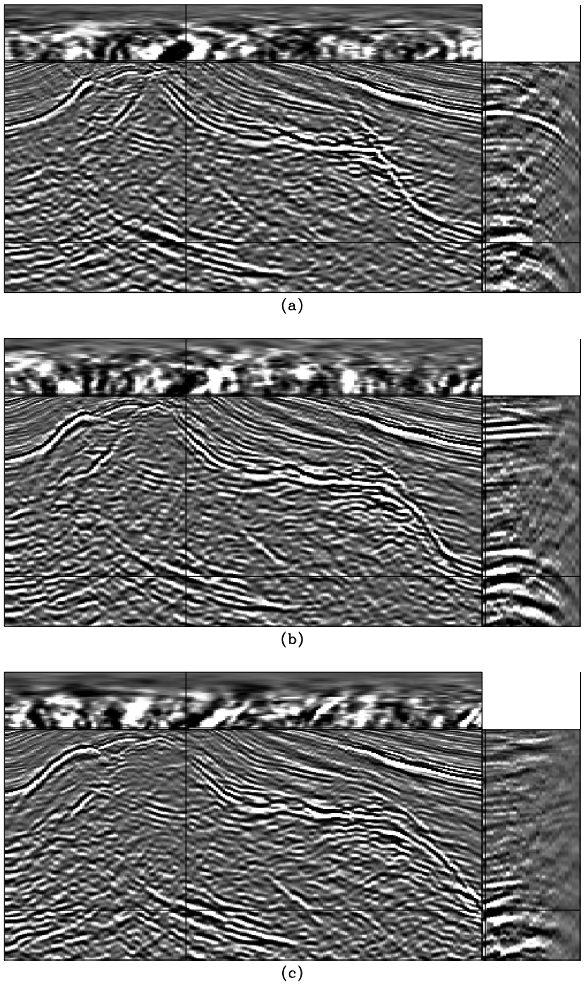

Figure 2: Angle-domain common-image gathers and effects of prestack Stolt residual migration for different ratios to the original velocity: 1.05 (a), 1.0 (b) and 0.95 (c).

Biondi, B., and Palacharla, G., 1996, 3-D prestack migration of common-azimuth data: Geophysics, **61**, no. 6, 1822–1832.

Biondi, B., and Sava, P., 1999, Wave-equation migration velocity analysis: 69th Annual Internat. Mtg., Soc. Expl. Geophys., Expanded Abstracts, 1723–1726.

Biondi, B., Fomel, S., and Chemingui, N., 1998, Azimuth moveout for 3-D prestack imaging: Geophysics, **63**, no. 2, 574–588.

Biondi, B., 1997, Azimuth moveout + common-azimuth migration: Cost-effective prestack depth imaging of marine data: 67th Annual Internat. Mtg., Soc. Expl. Geophys., Expanded Abstracts, 1375–1378.

Jacobs, J. A. C., Delprat-Jannaud, F., Ehinger, A., and Lailly, P., 1992, Sequential migration-aided reflection tomography: A tool for imaging complex structures: 62nd Annual Internat. Mtg., Soc. Expl. Geophys., Expanded Abstracts, 1054–1057.

Mosher, C. C., Foster, D. J., and Hassanzadeh, S., 1997, Common angle imaging with offset plane waves: 67th Annual Internat. Mtg., Soc. Expl. Geophys., Expanded Abstracts, 1379–1382.

O'Brien, M. J., and Etgen, J. T., 1998, Wavefield imaging of complex structures with sparse point-receiver data: 68th Annual Internat. Mtg., Soc. Expl. Geophys., Expanded Abstracts, 1365–1368.

Prucha, M., Biondi, B., and Symes, W., 1999, Angle-domain common-image gathers by wave-equation migration: 69th Annual Internat. Mtg., Soc. Expl. Geophys., Expanded Abstracts, 824–827.

Sava, P., 2000, Prestack Stolt residual migration for migration velocity analysis: 70th Annual Internat. Mtg., Soc. Expl. Geophys., Expanded Abstracts, submitted.

Stoffa, P. L., Fokkema, J. T., de Luna Freire, R. M., and Kessinger, W. P., 1990, Split-step Fourier migration: Geophysics, **55**, no. 4, 410–421.

Stolt, R. H., 1996, Short note–a prestack residual time migration operator: Geophysics, **61**, no. 02, 605–607.

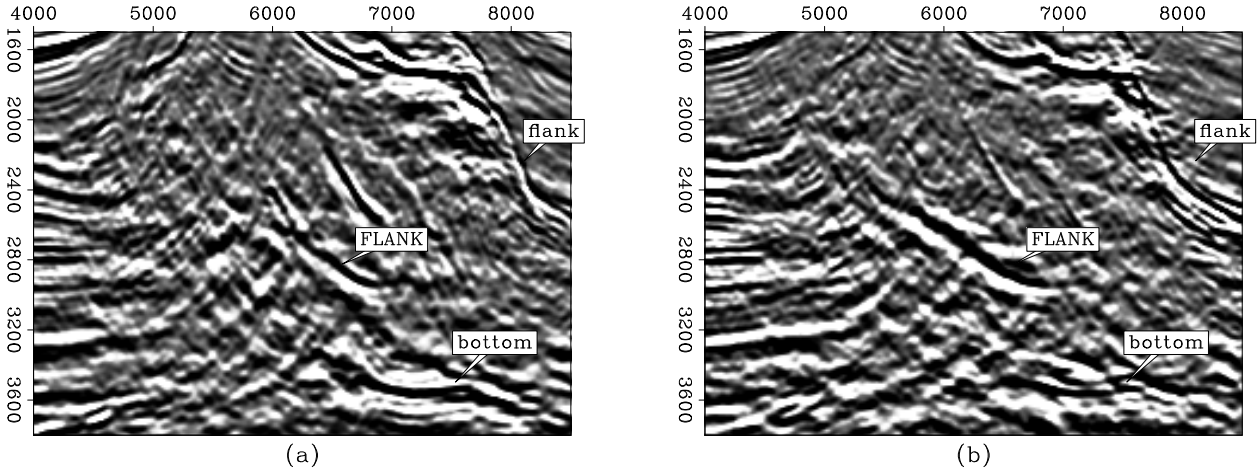

Figure 3: Image improvement with Stolt residual migration: (a) original migrated image and (b) image after residual migration with a ratio 1.05 to the original velocity model. The salt dome boundaries are designated on the image, which is a stack over all angles. The salt flank region on the left-hand side is enhanced.

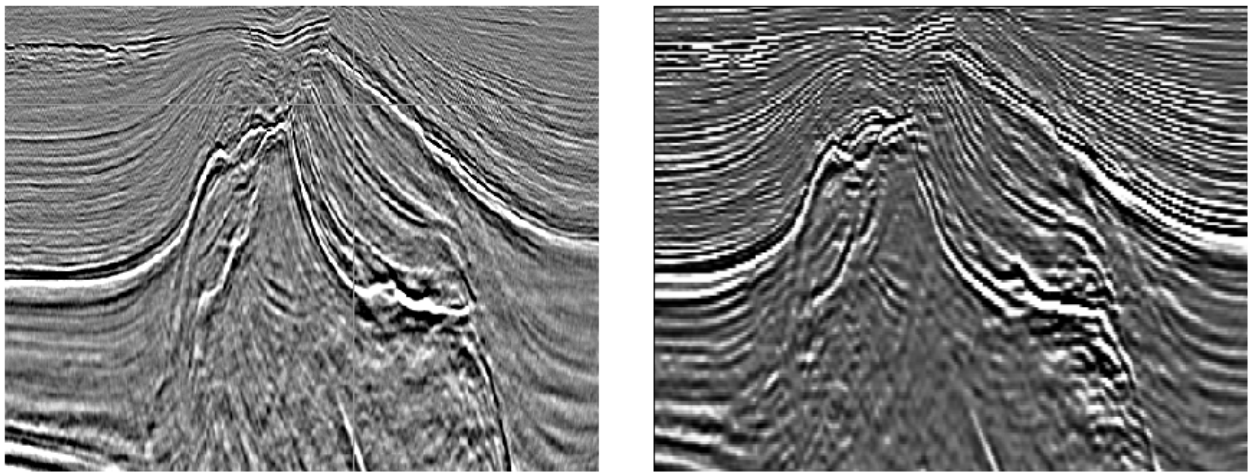

Figure 4: Comparison between Kirchhoff (left) and CAM (right) imaging results: close-up on the salt body in in-line section Cmp-Y=3250m.

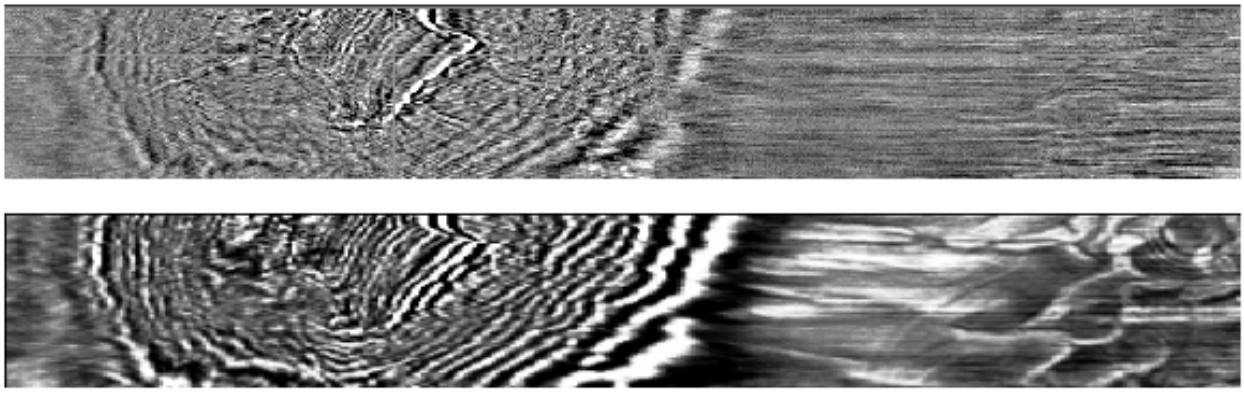

Figure 5: Comparison between Kirchhoff (top) and CAM (bottom) imaging results: depth slice at z=900m.